Hybrid, optical-computational, methodology for studies and optimization of microelectronic components

Cosme Furlong and **Ryszard J. Pryputniewicz**
NEST – NanoEngineering, Science, and Technology
CHSLT – Center for Holographic Studies and Laser micro-mechaTronics
Mechanical Engineering Department
Worcester Polytechnic Institute
Worcester, Massachusetts 01609-2280 USA

ABSTRACT

With the electronic industry being one of the most dynamic, in terms of new technologies, electronic packages have to be designed and optimized for new and ever more demanding applications in relatively short periods of time while satisfying electrical, thermal, and mechanical requirements, as well as cost and manufacturability. In addition, reliability and durability have to be taken into consideration. As a consequence, effective quantitative methodologies, such as optical and computational should be applied in the study and optimization of microelectronic components. In this paper, a hybridized use of nondestructive, noninvasive, remote, full field of view, quantitative opto-electronic holography techniques with computational modeling is presented. The hybridization is illustrated with a representative application, which shows that the combined use of opto-electronic holography techniques and computational modeling provides an effective engineering tool for nondestructive study and optimization of microelectronic components.

Keywords: deformation measurements, electronic packaging, electro-optic holography, fiber optics, hybrid methodology, microelectronic components, nondestructive testing, shape measurements.

1. INTRODUCTION

Figure 1 depicts an electronic printed circuit board (PCB), categorized as the second level of the electronic packaging hierarchy[1]. A PCB may contain a large number of electronic components (first level of electronic packaging) made of materials with different characteristics and properties and, therefore, each of the components behaving differently under specific loading conditions.

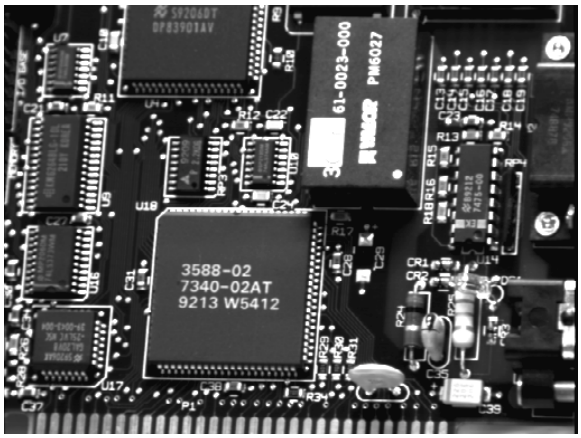

Fig. 1. Printed circuit board (PCB) corresponding to the second level of the electronic packaging hierarchy. The PCB is composed of a large number of electronic components (first level of electronic packaging), which have to reliably function in order to assure the correct functionality of an electronic package.

Under actual operating conditions the PCB as well as the individual electronic components, assembled on the PCB, are subjected to electromagnetic, electrical, thermal, and/or mechanical conditions of loading, which may generate failure of an electronic package. This failure can be due to any individual or a combination of the following mechanisms: fatigue, creep, stress relaxation, stress concentration, and/or bonding fractures[2,3]. In addition, failure can be induced by phenomena such as electromigration and popcorning[4-6]. Reliability of an electronic package depends on the correct functionality, under operating conditions, of the components at each one of the electronic packaging levels, starting from the first level. Therefore, due to the quantity of components assembled on an electronic package and the complexity of possible failure mechanisms, reliability assessment requires the application of effective quantitative methodologies. These quantitative methodologies comprise the optical and computational techniques[7-9].

An effective study and characterization of microelectronic components should include the use of both computational and experimental methodologies. Computational investigations enable parametric studies and the determination of critical engineering conditions, while experimental investigations, especially optical, provide qualitative and quantitative information on the actual response of the component of interest to the applied load conditions[9].

In this paper, a novel hybridized use of nondestructive, noninvasive, remote, full field of view, quantitative opto-electronic holography techniques with computational modeling is presented. The hybridization is illustrated with the investigation of a first level electronic packaging component, an electronic carbon resistor, showing that the combined use of quantitative optical techniques and computational modeling provides an effective engineering tool for nondestructive study and optimization of microelectronic components.

2. OPTICAL-COMPUTATIONAL METHODOLOGY

2.1. Experimental investigations

Figure 2 depicts a cross sectional view of a 3 ± 3 % ohm carbon resistor package of interest. In this resistor, the carbon-silica core is encapsulated in a silica shell package and two copper-lead leads are molded-in in order to provide connections to other components or to PCB. The resistor has nominal dimensions of 3.48 mm for the diameter and 10 mm for the length[10].

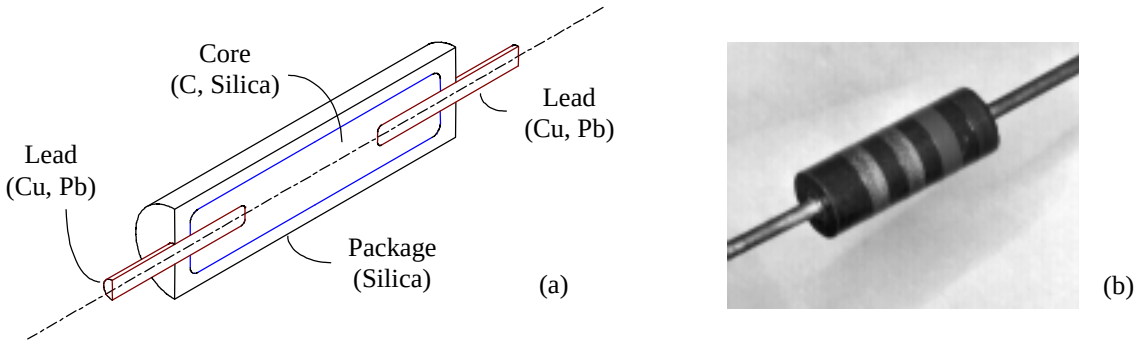

Fig. 2. Electronic carbon resistor of interest: (a) cross sectional view, and (b) actual package. The impedance of the resistor is 3 ± 3 % ohm.

The importance of testing the functionality of an electronic resistor is illustrated by comparing the electrical effects of two resistors in an electrical circuit: one in good operating condition and another in damaged condition. The damaged condition is produced by 15 sec overloading of the resistor. Figure 3 illustrate results of the testing procedures used to investigate the electrical effects of the resistor in an electronic circuit. Figure 3a depicts the measured frequency response (FR) of the circuit with the resistor in good operating condition, and Fig. 3b the measured FR of the circuit with the resistor in damaged condition. A periodic signal of 2 V_{pp} and 1 kHz was used as an input to the circuit. The undesirable noise observed in the FRs shown in Figs 3a and 3b, as compared to the FR of a pure 2 V_{pp}, 1 kHz signal, can be attributed to the effects of micro cracks developed in the core of the resistor as a result of imperfections in the manufacturing processes, and as a result of damage caused by overloading, respectively. Common testing procedures

used to study and quantify the level of damage consist of sectioning the components of interest and applying failure analysis, fractography, and microscopy techniques. However, these testing procedures are time consuming and destructive in nature[11].

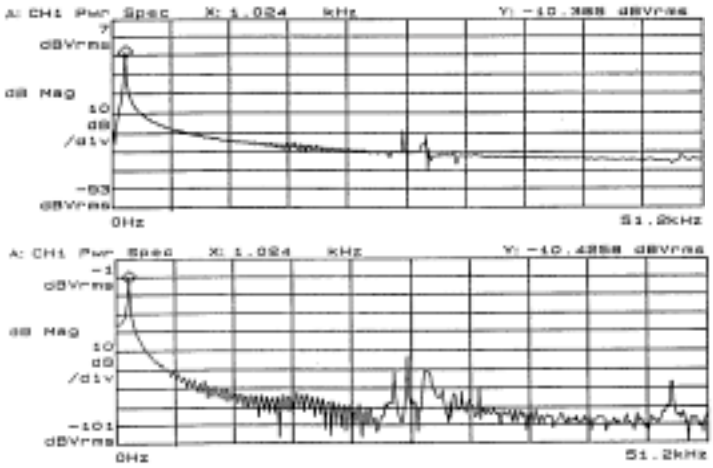

Fig. 3. Measured frequency responses of a testing circuit loaded with a pure 2 V_{pp}, 1 kHz signal with: (a) resistor in good operating condition and (b) resistor in damaged condition (overloaded). High frequency noise due to imperfections in the manufacturing processes (a), and as a result of damage caused by overloading (b), is observed.

For certain applications, the nondestructive testing (NDT) of electronic packages may be needed, especially for applications requiring noninvasive, full field of view, and real-time testing the behavior of a specific component subjected to actual operating conditions. This type of NDT can be accomplished by application of optical techniques and, in particular, speckle phase correlation techniques in the form of opto-electronic holography (OEH). Being noninvasive and providing qualitative and quantitative full field information are some of the main advantages of the OEH over other experimental techniques. With the OEH, it is possible to perform static and dynamic investigations of mechanical components subjected to a large variety of loading conditions. In addition, it is possible to measure the shape of components using optical contouring. Combination of these capabilities makes the OEH a powerful engineering tool that can be effectively utilized to study and optimize microelectronic components[9]. Recent technological advances in computer and fiber optic technologies have been applied to the OEH system and have added the possibility of using it in on-site investigations in order to study and diagnose problems in industrial environments[9,12].

2.1.1. Description of the experimental setup

Figures 4 and 5 depict the major components of a currently operational OEH system used for high resolution measurements of shape and deformation/displacement vectors in static and dynamic investigations[9,12]. The light source is an infrared MOPA (Master Oscillator/Power Amplifier) laser diode (LD), wavelength tunable with an operational wavelength centered at 994 nm (at 25 ^{o}C), thermoelectric cooling capabilities, horizontal linearly polarized output, driven by the controller LDD, Fig. 4. The output of the LD is directed through a Faraday optical isolator (OI) providing back reflection isolation to – 41 dB. The OI provides 47^{o} rotation at 994 nm and the polarizer on its input side is set to horizontal polarization in order to match the main polarization axis of the LD output. After the OI, light is launched into a single mode fiber optic directional coupler assembly, FA, Fig. 5, by means of a laser to fiber coupler (LFC), which is comprised of a GRIN lens, a 5 degrees of freedom stage, and an FC/AP connector port. The main components of the FA are three single mode fiber optic directional couplers (DC1, DC2, DC3), four piezoelectric cylinders (PZT1, PZT2, PZT3, PZT4), and FC connectorized I/O's. Table 1 summarizes the major features of the FA.

Table 1. Major features of the single mode fiber optic directional coupler assembly, FA.

Input port	Application	Mode
I_1	One illumination and three reference beams	Three-camera
I_2	One reference and three illumination beams	Three-illumination
I_2	Four illuminations	In-plane speckle correlation

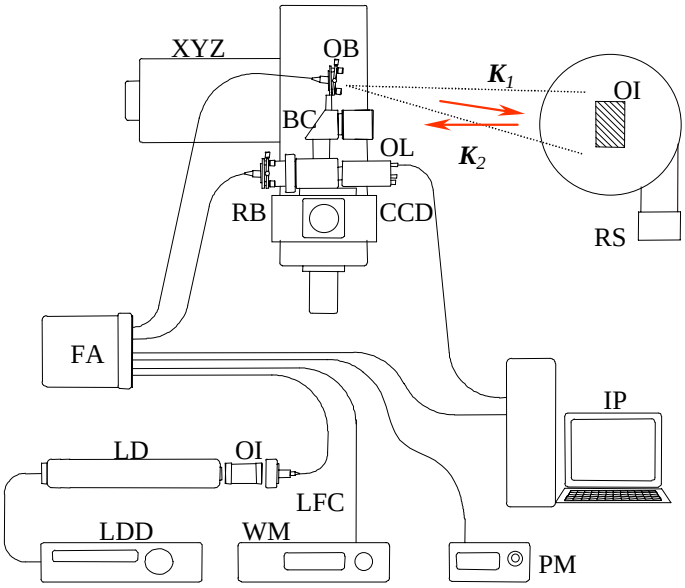

Fig. 4. Fiber-optic-based OEH setup arranged to perform high-resolution shape and deformation measurements: LDD is the laser diode driver, LD is the laser diode, OI is the optical isolator, LFC is the laser to fiber coupler, WM is the optical wavelength meter, PM is the optical power meter, IP is the image processing computer, FA is the single mode fiber optic directional coupler assembly, RB is the FC connectorized reference beam, CCD is the CCD camera, OL is the objective lens, BC is the beam combiner, XYZ is the X-Y-Z translational stage, OB is the FC connectorized object beam, RS is the rotary stage, and OI is the object under investigation. $\boldsymbol{K}_1$ and $\boldsymbol{K}_2$ are the illumination and observation direction vectors, respectively.

The experimental arrangement shown in Fig. 4 is configured in the mode with one illumination and three reference beams. In this mode, the higher output beam from the FA is utilized as the object beam (OB) to illuminate the object of interest (OI), and one of the lower output beams is used as the reference beam (RB). Object and reference beams are recombined in the beam combiner (BC), and the resultant irradiances are transferred to the image processing computer (IP) through the use of a CCD camera. The two additional lower output beams are utilized for monitoring the optical characteristics of the LD. Specifically, one of the lower output beams is utilized as input to the optical wavelength meter (WM), providing absolute wavelength measurements with a resolution of 0.0001 nm, and the other lower output beam is utilized for monitoring the optical power of the LD. For this particular configuration, the ceramic piezoelectric cylinder PZT1 (Fig. 5) is controlled by the IP and used for application of phase-stepping algorithms. In addition, the ceramic piezoelectric cylinder contained in the RB can be utilized for quantitative analysis in dynamic, or time-average, investigations requiring characterization of both shape and dynamically induced deformations[9].

In Fig. 4, the BC, OB, OL, CCD, RB, and required hardware are mounted on a mechanical fixture (interferometric head, IH), which in turn is assembled onto an X-Y-Z translational stage, with each axis having an independent positioning resolution of 0.1 μm. The object of interest OI is mounted on a rotary stage RS having an angular positioning resolution of $5 \cdot 10^{-5}$ deg.

With the OEH shown in Fig. 4, it is possible to measure deformation and shape of components of interest using the same experimental setup. High-resolution absolute shape measurements are made using the two wavelengths technique[12].

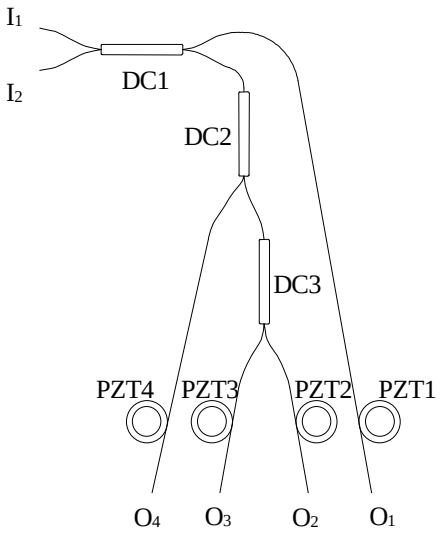

Attenuation, dB

I_1-O_1 = 1.10	I_2-O_1 = 1.10
I_1-O_2 = 10.9	I_2-O_2 = 10.9
I_1-O_3 = 10.9	I_2-O_3 = 10.9
I_1-O_4 = 11.7	I_2-O_4 = 11.7

Splitting, %

I_1	I_2	
80	20	O_1
7	28	O_2
7	28	O_3
6	24	O_4

Fig. 5. Single mode fiber optic based directional coupler assembly (FA): I_1 and I_2 are the FC connectorized input fibers, DC1, DC2, and DC3 are the directional couplers, PZT1, PZT2, PZT3, and PZT4 are the ceramic piezoelectric cylinders, and O_1, O_2, O_3, and O_4 are the FC connectorized output fibers.

2.1.2. Static double-exposure investigations

In the OEH, optical path length changes, related to mechanical deformations/displacements in static investigations, are evaluated from interference patterns of object and reference beams having complex light fields $F_o(u,v)$ and $F_r(u,v)$, with (u,v) representing the discrete coordinates defining the image plane of the CCD camera. After beam splitting, and considering phase stepping, irradiance of the combined wavefronts corresponding to the n-th phase step and characterized by the wave number $2\pi/\lambda$, is described by[13]

$$\begin{aligned} I_n(u,v) &= [F_o(u,v) + F_r(u,v)][F_o(u,v) + F_r(u,v)]^*, \\ &= I_B(u,v) + I_M(u,v)\cos[\Delta\phi(u,v) + \theta_n], \end{aligned} \tag{1}$$

where

$$I_B(u,v) = I_o(u,v) + I_r(u,v), \tag{2}$$

is the background irradiance, and

$$I_M(u,v) = 2[I_o(u,v)\cdot I_r(u,v)]^{1/2}, \tag{3}$$

is the modulation irradiance. In Eqs 1 to 3, $I_o(u,v)$ and $I_r(u,v)$ are the observed and reference beam irradiances, respectively; $\Delta\phi(u,v) = \phi_o(u,v) - \phi_r(u,v)$, with $\phi_o(u,v)$ representing a random phase due to light scattering from the object of interest and $\phi_r(u,v)$ representing a uniform phase from a smooth reference beam wavefront; and θ_n is the applied n-th known phase step appropriately calibrated for the optical wavelength λ. To facilitate static investigations,

the argument of the periodic term of Eq. 1 is modified to include the phase change due to static deformations/displacements of the object of interest subjected to specific loading and boundary conditions. This phase change is characterized by the fringe-locus function Ω, constant values of which define fringe loci on the surface of the object, and, observed at point (u,v) of the detector, it is defined as[14,15]

$$\Omega = (\boldsymbol{K}_2 - \boldsymbol{K}_1) \cdot \boldsymbol{L} = \boldsymbol{K} \cdot \boldsymbol{L} \ , \tag{4}$$

where $\boldsymbol{K}_1$ and $\boldsymbol{K}_2$ are the vectors of illumination and observation, respectively, $\boldsymbol{K} = \boldsymbol{K}_2 - \boldsymbol{K}_1$ is the sensitivity vector, and $\boldsymbol{L}$ is the displacement vector. Therefore, the detected irradiances resulting from the combined observed and reference beam irradiances are described by

$$I_n^{'}(u,v) = I_B(u,v) + I_M(u,v)\cos[\Omega(u,v) + \Delta\phi(u,v) + \theta_n] \ . \tag{5}$$

Since it is Ω that carries information pertaining to variations of the optical path length, the OEH video frame processing algorithms eliminate $\Delta\phi$ from the argument of the periodic function of the irradiance distributions given in Eqs 1 and 5, yielding an image that has intensity modulated by a periodic function with Ω as the argument[15].

The OEH can work in display and data mode. In the display mode, interference patterns are observed at video rate speed and are modulated by a cosinusoidal function of the form

$$4I_M(u,v)\cos[\Omega(u,v)/2] \ , \tag{6}$$

which is obtained by performing specific algebraic operations between frames acquired at the two different states of deformation, described by Eqs 1 and 5, respectively. This mode is used for adjusting the OEH system and for qualitative investigations. The data mode is used for performing quantitative investigations. In the data mode, two additional images are generated: a cosinusoidal image,

$$D(u,v) = 16I_M^2(u,v)\cos[\Omega(u,v)] \ , \tag{7}$$

and a sinusoidal image,

$$N(u,v) = 16I_M^2(u,v)\sin[\Omega(u,v)] \ , \tag{8}$$

which are processed simultaneously to produce quantitative results by computing

$$\Omega(u,v) = \tan^{-1}\left[\frac{N(u,v)}{D(u,v)}\right] . \tag{9}$$

From Eq. 9 it can be observed that the spatial phase distribution represented by $\Omega(u,v)$ is a discontinuous function wrapped modulo 2π, which must be further processed in order to obtain a continuous spatial phase distribution by application of phase-unwrapping algorithms.

Accurate measurements of optical path length changes, characterized by displacement vector $\boldsymbol{L}$, are obtained by[9]:

1) accurate determination of the continuous spatial phase distribution $\Omega(u,v)$, which in turn depends on:

   a) the accuracy in the image acquisition process, for which low noise in the CCD camera and relating signal conversion and processing boards are required

   b) the appropriate calibrated phase-stepping algorithm for generation of speckle correlation interferograms and data images

c) the effective processing of $\Omega(u,v)$ modulo 2π;

2) determination of the magnification factors M_u and M_v, which allow the transformation from image plane coordinates (u,v) to actual global coordinates system (x,y) as $(M_u \cdot u, M_v \cdot v) \rightarrow (x,y)$. In the OEH setup shown in Fig. 4, magnification factors are measured using the X-Y-Z translational stage in combination with image processing procedures;

3) calibration and characterization of the camera and imaging system. This characterization allows the accurate determination of the points of observation and illumination, which are utilized to evaluate the sensitivity vector ***K***. The camera calibration methods used for characterizing the imaging metrics in the OEH system shown in Fig. 4 utilize *NIST* (National Institute of Standards and Technology[16]) traceable gages.

2.1.3. NDT of electrical resistors

Figure 6 depicts external appearance of the resistors tested and typical interferograms corresponding to the real-time investigations of the resistors, in good and damaged operating conditions, using the static double-exposure acquisition mode. Resistors were tested with an OEH setup characterized by a vector ***K*** sensitive to the out-of-plane component of deformation, while loaded with a 2 V_{pp}, 1 kHz periodic signal. The larger number of interference fringes observed in Fig. 6c (damaged condition) than in Fig. 6b (good condition) clearly indicates that the resistors have significantly different behavior under the same loading conditions, therefore, illustrating the applicability of the OEH technique for health monitoring, in real-time, of electronic packages. Quantitative characterization of structural deformations due to thermal fields induced by electric loads can be obtained with OEH techniques. Figure 7 shows typical results corresponding to the fringe analysis of data images associated with Fig. 6b.

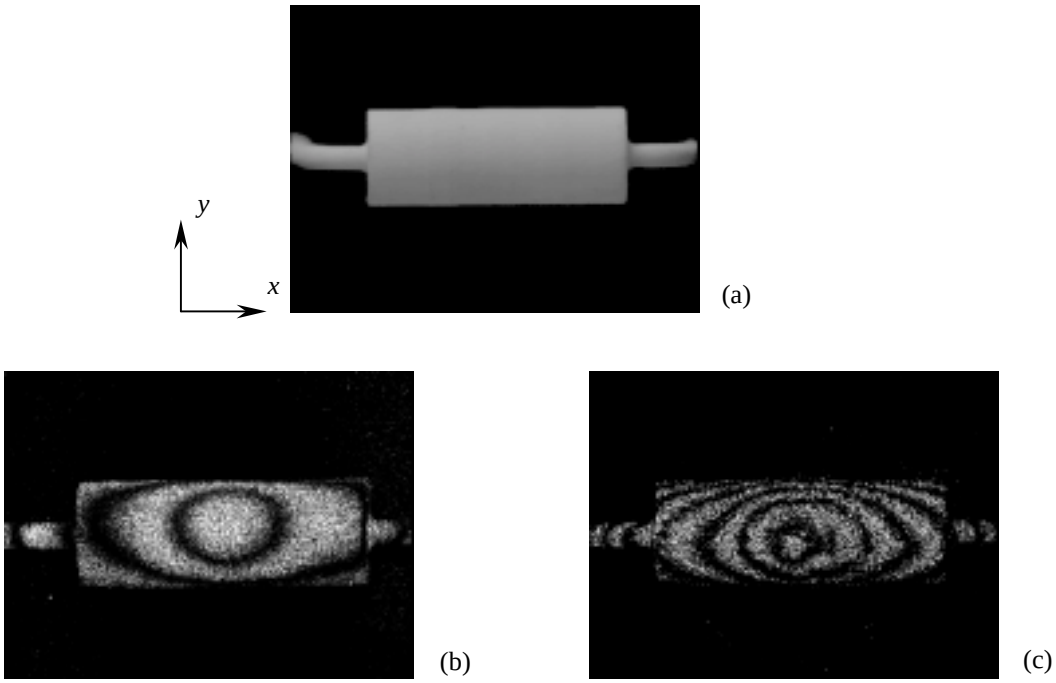

Fig. 6. Real-time NDT investigation of electronic resistors using OEH: (a) external appearance as observed on the OEH video display, (b) interferogram of a resistor in good operating condition, and (c) interferogram of a resistor in damaged condition. Experimental setup was sensitive to the out-of-plane component of deformation. Resistors were loaded with a 2 V_{pp}, 1 kHz periodic signal.

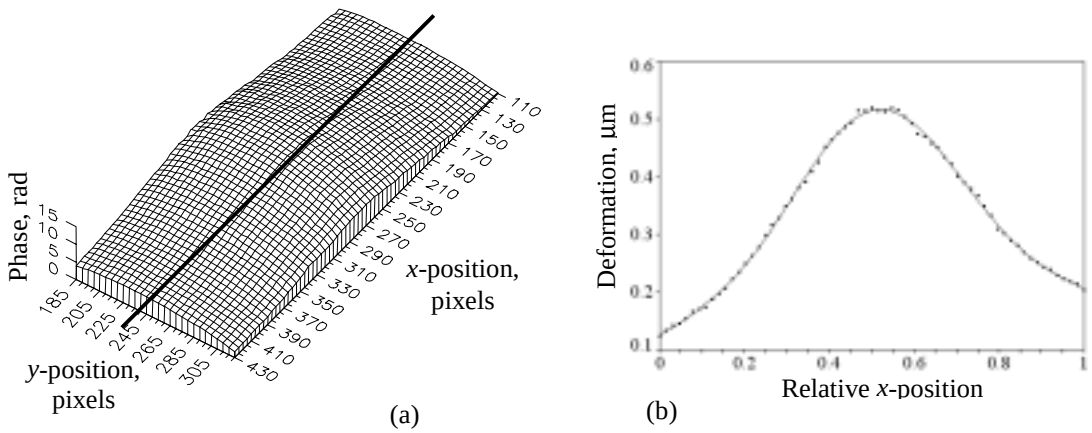

Fig. 7. Electrically induced displacements characterized using OEH techniques. Measured radial displacement U_r from data images corresponding to Fig. 6b: (a) out-of-plane spatial phase distribution of the resistor based on quantitative OEH investigations, and (b) radial displacement along the line shown in (a), indicating maximum radial displacement of 0.52 µm obtained with accuracy better than 0.005 µm.

2.2. Computational modeling

An electrical resistor is introduced into an electronic circuit in order to provide a specific voltage difference. This voltage difference induces heat in the resistor and, therefore, temperature changes that produce mechanical strains and thus mechanical stresses, which may produce undesirable mechanical failure. The behavior of the resistor can be analyzed by considering electromagnetic, thermal, and mechanical stress-strain effects[9,17]. An initial investigation consists of studying a linear and steady-state loading condition. Therefore, computationally, it is necessary to solve the electric potential equation

$$\nabla \cdot \left(\bar{\kappa} \nabla V\right) = 0 \ , \tag{10}$$

where $\bar{\kappa}$ is the electrical conductivity of the material, and V is the spatially varying electrical potential. Solution of Eq. 10 allows evaluation of Joule's heat generated, $Q = \bar{\kappa} \mid \nabla V \mid^2$, and determination of spatially dependent temperature field T by solving the thermal equilibrium equation

$$\nabla(\tilde{k} \nabla T) + Q = 0 \ , \tag{11}$$

in which $\tilde{k}$ is the thermal conductivity of the material. Solution of Eq. 11 can be applied to the strain-displacement elasticity equations and to the solution of the stress-strain equilibrium equation

$$\sigma = E\left(\varepsilon + \alpha \Delta T\right) \ , \tag{12}$$

where σ is the thermo-mechanical stress tensor, E is the modulus of elasticity of the material, ε is the mechanical strain tensor, α is the coefficient of thermal expansion of the material, and ΔT is the temperature difference between the temperature obtained by solving Eq. 11 and an ambient temperature T_o. Solutions of Eqs 10 to 12 can be obtained by finite element method (FEM) modeling[9]. Figure 8 shows the half cross sectional FEM solution for the radial deformation induced by a 2 V load indicating a maximum predicted radial deformation of 1.22 µm. Symmetry was assumed and boundary conditions similar to operating conditions of a resistor were used. Material properties were obtained from published data. By comparing experimental and computational results for the radial deformation, Figs 7b and 8b, differences between measured and predicted results are realized, which indicate that any further computational investigations would yield erroneous results.

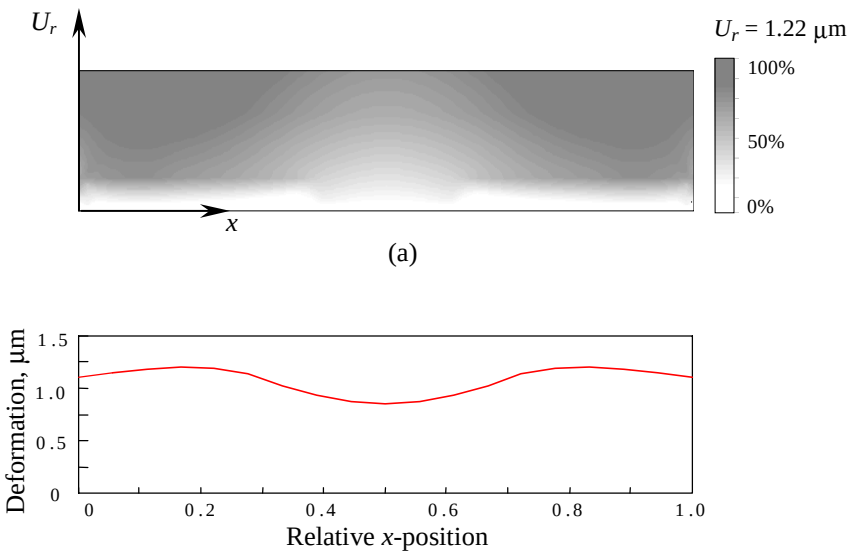

Fig. 8. Half cross sectional FEM model of resistor predicting electrically induced radial deformations: (a) cross sectional radial deformation field distribution U_r and (b) deformation along a longitudinal external surface of the resistor.

2.3. Improvement of results: hybrid methodology

Figure 9 depicts a flowchart of the hybrid, optical and computational, methodology applied to the investigation of microelectronic components[7-9,18]. According to Fig. 9, computational investigations are performed on the initial configuration, while the actual component is tested experimentally. Comparisons between experimental and computational results are based on fringe prediction (FP).

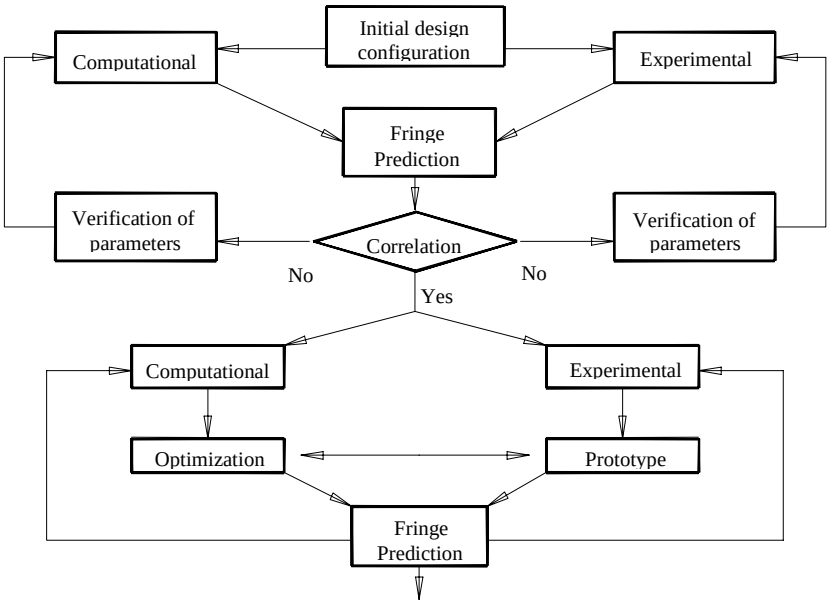

Fig. 9. Hybrid, optical and computational, methodology applied to the investigation of microelectronic components.

When discrepancies between computational and experimental results are encountered, it is necessary to verify the input parameters for the computational model and or experimental conditions. Verifications include uncertainty and analytical investigations, characterization of material properties, geometric and modeling accuracy, mechanical and optical setups, and/or the use of experimentally obtained boundary conditions in the computational models. The results of these comparisons provide information on the accuracy of the computational analyses with respect to modeling the experimental behavior of the component of interest. When an acceptable degree of accuracy is obtained, the computational model is applied to perform sensitivity analyses of the selected objective function with respect to the specified design variables as well as shape optimization of the initial configuration. The geometry obtained from the shape optimization analyses is used to manufacture a prototype, which is experimentally tested in order to perform computational and experimental comparisons through the FP operation.

Figure 10 shows FP results before and after the application of the hybrid methodology. Predicted fringe pattern depicted in Fig. 10a corresponds to FEM modeling results shown in Fig. 8, and the fringe pattern shown in Fig. 10b corresponds to the FEM results obtained after application of the hybrid methodology. Improvements are mainly due to the utilization of experimentally obtained material properties in the computational model. The predicted patterns should be compared to measured interference pattern, Fig. 6b, to realize improvements in the results.

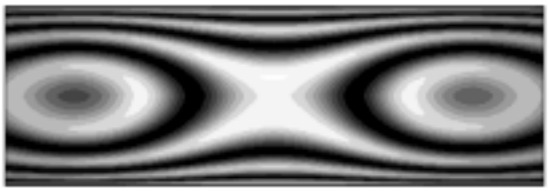

(a)

(b)

Fig. 10. Predicted fringe patterns corresponding to electrically induced deformations on electrical resistors: (a) before and (b) after hybrid methodology. Comparisons with measurements, Fig. 6b, indicate improvements in the results.

3. CONCLUSIONS

A hybrid optical-computational methodology for nondestructive testing of microelectronic components has been presented and illustrated with a representative application. This application clearly demonstrates that neither only computational nor only experimental techniques should be applied to solve an engineering problem, because applying only one of the techniques can provide erroneous information. Using this hybrid approach, displacements and strains are determined with accuracies better than 0.01 μm and 0.000,05 %, respectively, and provide indispensable data for testing and development of reliable electronic packages.

4. ACKNOWLEDGEMENTS

The authors would like to thank all members of the NEST/CHSLT for their helpful discussions and assistance during preparation of this paper.

5. REFERENCES

1. P. Engel, "Experimental structural analysis topics in printed circuit board systems," *Proc. SEM*, 215-217, 1995.

2. A. Dasgupta and M. Pecht, "Material failure mechanisms and damage models," *IEEE Transactions on Reliability*, **40**(5):531-536, 1991.

3. A. Dasgupta, "Failure mechanism models for cyclic fatigue," *IEEE Transactions on Reliability*, **42**(4):548-555, 1993.

4. D. Young and A. Christou, "Failure mechanism models for electromigration," *IEEE Transactions on Reliability*, **43**(2):186-192, 1994.

5. P. Lall, "Tutorial: temperature as an input to microelectronics – reliability models," *IEEE Transactions on Reliability*, **45**(1):3-9, 1996.

6. A. A. Gallo and R. Munamarty, "Popcorning: a failure mechanism in plastic-encapsulated microcircuits," *IEEE Transactions on Reliability*, **44**(3):362-367, 1995.

7. C. Furlong and R. J. Pryputniewicz, "Hybrid, experimental and computational, investigation of mechanical components," *Proc. SPIE*, **2861**:13-24, 1996.

8. C. Furlong and R. J. Pryputniewicz, "Hybrid computational and experimental approach for the study and optimization of mechanical components," *Opt. Eng.*, **37**(5):1448-1455, 1998.

9. C. Furlong, *Hybrid, experimental and computational, approach for the efficient study and optimization of mechanical and electro-mechanical components*, Ph.D. Dissertation, Worcester Polytechnic Institute, Worcester, MA, 1999.

10. C. Furlong and R. J. Pryputniewicz, "Nondestructive damage evaluation of electro-mechanical components using a hybrid, computational and experimental, approach," *Proc. Mat. Res. Soc.*, **591**:111-116, 1999.

11. I. J. Goldstein, E. D. Newburn, P. Echin, C. D. Joy, C. Fiori, and E. Lifshin, *Scanning electron microscopy and X-ray microanalysis*, Plenum Press, New York, 1984.

12. C. Furlong and R. J. Pryputniewicz, "Absolute shape measurements using high-resolution optoelectronic holography methods," *Opt. Eng.*, **39**(1):216-223, 2000.

13. B. E. A. Saleh and M. C. Teich, *Fundamentals of photonics*, Wiley, New York, 1991.

14. C. M. Vest, *Holographic interferometry*, Wiley, New York, 1979.

15. R. J. Pryputniewicz, *Holographic numerical analysis*, Worcester Polytechnic Institute, Worcester, MA, 1992.

16. http://www.nist.gov

17. A. Shadowitz, *The electromagnetic field*, Dover Publications, New York, 1988.

18. R. J. Pryputniewicz, "A hybrid approach to deformation analysis," *Proc. SPIE*, **2342**:282-296, 1994.
